scisearch INTERNATIONAL PEER-REVIEWED JOURNALS

RESEARCH PAPER

Factor-Graph Smoothing with Thermodynamics-Consistent Latent States for Dissolution-Buffered Kick Diagnosis under Intermittent Telemetry

Andres Patiño[1] and Felipe Cardona[1]

[1]Universidad de la Amazonia, Avenida Circunvalar 1-1, Florencia 180002, Caquetá, Colombia
[2]Universidad de los Llanos, Kilómetro 12 Vía Puerto López, Vereda Barcelona, Villavicencio 500017, Meta, Colombia

Abstract
Drilling operations that rely on managed pressure drilling increasingly depend on rapid interpretation of surface measurements while maintaining tight safety margins. The difficulty is amplified by persistent actuation at the choke and pumps, which induces transients that can resemble influx signatures, and by limited downhole observability that forces decisions to be made under structural ambiguity. In oil-based and synthetic-based fluids, gas can partially dissolve and induce swelling of the circulating liquid, shifting the relationship among pit-volume trends, pressures, and actual free-gas inventory in the annulus. This paper develops a factor-graph state estimation and decision layer that explicitly represents dissolution and swelling as latent thermodynamics-constrained states, while accommodating intermittent telemetry and sensor outages. The technical contribution is a sparse smoothing formulation that couples one-dimensional annular hydraulics summaries with a bounded thermodynamic partition model, encoded as inequality-constrained factors and thermodynamic-consistency priors, enabling stable inference when measurements are sparse, biased, and temporally correlated. A hybrid variational–Laplace inference scheme is derived to preserve positivity and phase-fraction bounds without nonphysical clipping, and an event-triggered telemetry policy is co-designed to maximize expected information gain subject to bandwidth constraints. The approach yields posterior distributions for free and dissolved gas inventories and for safety-relevant outputs, and it produces diagnostics that distinguish swelling-consistent pit gain from free-gas-driven compressibility signatures using posterior geometry rather than heuristic thresholds. Numerical experiments demonstrate improved ambiguity resolution under realistic actuation, closure uncertainty, and bias drift, with inference remaining stable under long telemetry gaps.

1. Introduction

Early detection and characterization of gas influx is an estimation problem embedded in a control loop (1). Under managed pressure drilling, surface backpressure and flow regulation reduce the amplitude of excursions but increase the complexity of signal interpretation, because deliberate actuation introduces structured transients and because the mapping from downhole states to surface observables changes with both control and state. The operational environment therefore exhibits three features that are difficult to reconcile with classic threshold logic: nonstationary inputs, partial observability of distributed states, and strong coupling between unobserved thermodynamic partitioning and observed volumetric signals. When these features interact, an algorithm that excels in steady hydraulics can fail in transient regimes, and an algorithm tuned for one fluid system can misinterpret another because dissolution and swelling alter the effective constitutive behavior of the circulating system.

A central ambiguity arises from the existence of multiple internal explanations for similar surface patterns. Pit gain is frequently treated as a signature of free gas entering the wellbore, yet pit gain is a volumetric observation that can be influenced by density changes, compressible storage, instrument bias, and swelling. Under oil-based and synthetic-based fluids, dissolution can absorb part of the invading gas mass into the liquid and thereby increase the liquid volume through swelling while delaying free-gas dominance (2). In such conditions, early pit gain can be real and operationally important while still being weakly informative about near-term surface free-gas handling. A decision layer that conflates pit gain with free-gas holdup can therefore overpredict immediate surface risk and underpredict alternative constraints such as pit capacity and density-driven pressure margins.

The present paper argues that this ambiguity is best addressed as a structured smoothing problem rather than as a sequence of independent residual tests. The smoothing viewpoint treats all measurements, controls, and latent states over a horizon as a joint probabilistic object. It becomes possible to represent not only the forward dynamics but also thermodynamic relationships as constraints in the probabilistic model, and it becomes possible to fuse intermittent telemetry without relying on ad hoc resets. This is operationally relevant because downhole telemetry is often intermittent, delayed, or absent during critical windows, and because the estimation problem must remain numerically stable through those gaps (3). A factor-graph formulation is particularly suited to this setting because it naturally accommodates asynchronous sensors, delayed

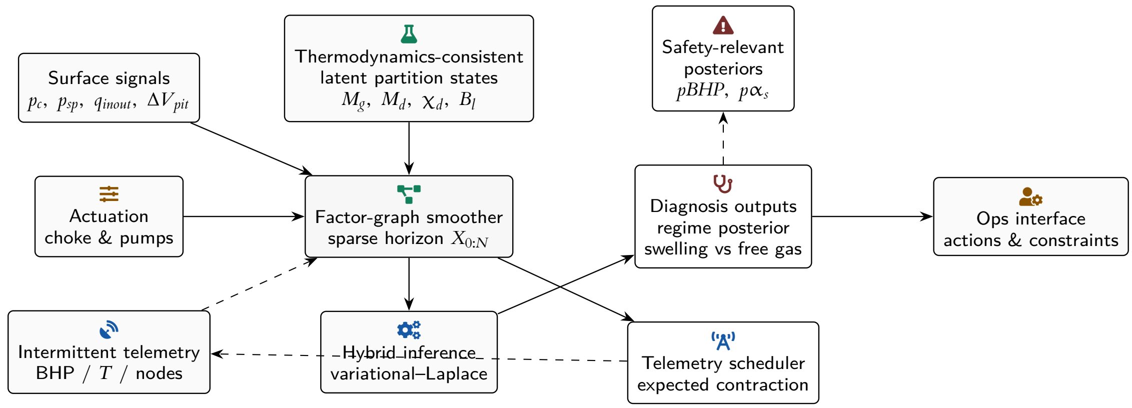

Figure 1. End-to-end diagnosis stack under intermittent observability. Surface measurements and structured actuation are fused by a sparse factor-graph smoother whose state explicitly partitions free and dissolved gas and enforces bounded swelling behavior. A hybrid variational–Laplace layer yields physically admissible posteriors used for regime-sensitive diagnostics and an event-triggered telemetry policy that prioritizes packets when ambiguity is high.

Table 1. Key latent state variables in the reduced annular representation used for factor-graph smoothing.

Symbol	Description	Units / scale
$pt \in \mathbb{R}^{n_p}$	Pressure nodes along the annulus	MPa, bar
qt	Mixture volumetric flow proxy	m^3/s
$M_g t$	Integrated free-gas mass in annulus	kg
$M_d t$	Integrated dissolved-gas mass in liquid	kg
$\alpha_s t$	Near-surface free-gas proxy	0–1 (fraction)
$\chi_d t = M_d M_l$	Normalized dissolved fraction	0–1 (fraction)
$M_l t$	Effective liquid mass over horizon	kg

factors, and heterogeneous uncertainty models, while exploiting sparsity to remain computationally tractable.

Thermodynamic closure is not introduced here as a standalone contribution, but as a necessary ingredient for a latent-state model that can separate swelling-driven and free-gas-driven regimes. In this context, Manikonda et al. (2020) (4) introduced an early thermodynamic modeling framework that quantified how gas can dissolve into oil-based drilling fluids during a kick and how that dissolution can be linked to volumetric behavior relevant to operational interpretation. The present work leverages that conceptual pathway by embedding a bounded, thermodynamics-consistent partition state into the estimator, not to reproduce a full equation-of-state solver online, but to enforce the qualitative and quantitative constraints that make swelling a plausible explanation for observed signals.

A second limitation in real-time inference is uncertainty in fluid properties and correlations (5). Gas density, viscosity, and other properties influence hydrostatic gradients and frictional losses, and small systematic errors in these properties can lead a state estimator to compensate by biasing inferred influx rates or by distorting inferred holdup distributions. This is particularly problematic when the estimator is tuned to fit pressure data tightly, because pressure is both safety critical and highly sensitive to closure mismatch when integrated over long annular lengths. Empirical assessments indicate that correlation errors at the few-percent level can persist even for comparatively accurate models in high-temperature and high-pressure regimes (6). Such error levels are small enough to be ignored in static calculations yet large enough to perturb transient inference and to cause spurious confidence if not represented as uncertainty in the model.

The thesis of the paper is that a factor-graph smoother with thermodynamics-consistent latent variables and explicit bias states can provide a stable and interpretable diagnosis layer for dissolution-buffered kicks under intermittent telemetry. The technical contribution is a computationally tractable inference method that (i) represents free and dissolved gas inventories as separate but coupled latent states, (ii) enforces physically

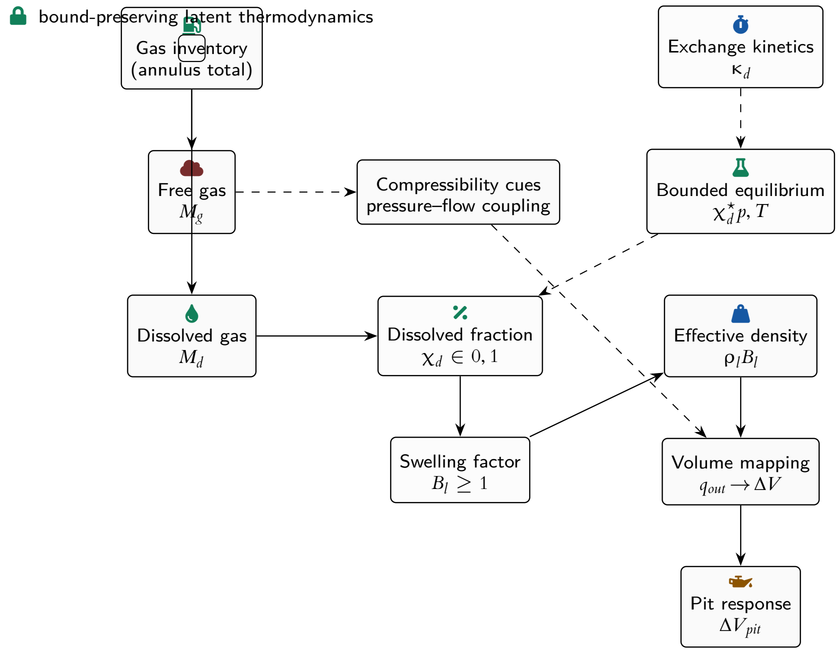

Figure 2. Latent partitioning and swelling pathway used to resolve pit-gain ambiguity. The estimator separates free-gas mass M_g from dissolved mass M_d and constrains dissolved fraction χ_d through bounded equilibrium trends and exchange kinetics priors. Swelling B_l modifies effective density and volumetric return mapping, allowing pit-volume growth to be explained by dissolution-consistent swelling when pressure–flow compressibility cues do not support free-gas dominance.

meaningful bounds and monotone thermodynamic consistency through constrained factors, (iii) accommodates asynchronous and intermittent measurements through factor scheduling and robust likelihoods, and (iv) co-designs telemetry triggering with the smoother to maximize expected information gain about safety-relevant latent quantities (7). The contribution is independent of any specific commercial hydraulics simulator; the estimator is designed around structural constraints and sparse inference rather than around high-fidelity forward modeling.

The remainder of the paper proceeds as follows. The next section introduces a reduced but physically anchored state representation for annular hydraulics and partitioned gas inventory, along with the measurement model and uncertainty structure needed for smoothing. The following section formulates the factor graph and derives the sparse optimization problem corresponding to maximum a posteriori estimation, highlighting how thermodynamic constraints and inequality bounds are encoded as factors. The next section develops inference algorithms, including a hybrid variational–Laplace approach that preserves bounds without clipping and yields calibrated uncertainty. The subsequent section introduces an event-triggered telemetry policy that is optimized with respect to expected posterior contraction and that integrates naturally with the factor-graph structure (8). The final technical section reports numerical experiments and ablation analyses, and the paper concludes with implications, limitations, and extensions.

2. Reduced State Representation with Partitioned Gas Inventory and Measurement Uncertainty

A full annular multiphase model with detailed slip, cuttings transport, and thermal coupling is rarely identifiable from surface measurements alone, and it can be too expensive for repeated optimization inside a smoother. The objective here is therefore not to maximize forward fidelity, but to select a state that captures the couplings that dominate the measured signals and the safety-relevant quantities under managed pressure operation. The state must be expressive enough to represent dissolution buffering and swelling, and it must be compatible with sparse inference across time.

The annulus is represented by a one-dimensional coordinate $z \in 0, L$ with a coarse spatial summarization. Pressure is represented by a vector of node values $pt \in \mathbb{R}^{n_p}$ at selected depths, chosen to capture hydrostatic structure and dominant frictional segments. Flow is represented by a mixture volumetric flow proxy qt and a compressible storage proxy that captures the time constant of pressure response under boundary actuation (9). Gas inventory is partitioned into a free component and a dissolved component, represented by coarse inventories rather than detailed distributions. Specifically, define $M_g t$ as an integrated free-gas mass in the annulus and $M_d t$ as an integrated dissolved-gas mass carried by the liquid. A near-surface free-gas proxy $\alpha_s t$ is included to represent surface handling risk and to capture the fact that surface gas rate depends not only on total free-gas mass but also on its distribution.

The dissolved inventory influences the system through swelling. Swelling modifies effective liquid density and specific volume, thereby changing hydrostatic head and the mapping

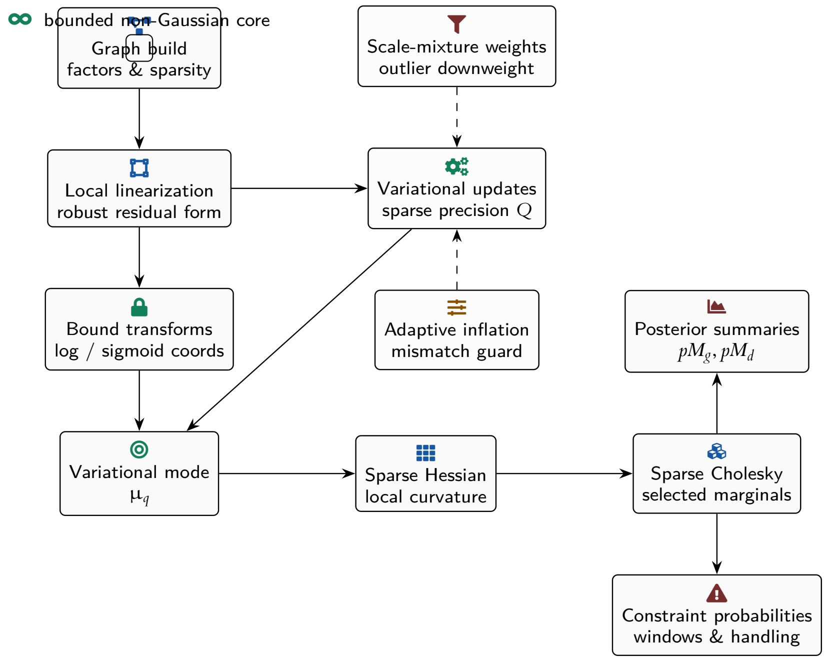

Figure 3. Hybrid variational–Laplace inference for bound-preserving uncertainty. Nonlinear factors are linearized locally while constrained variables are represented in unconstrained coordinates to keep posteriors physically admissible. Robust scale-mixture weights mitigate outliers, and adaptive inflation protects against closure mismatch. A Laplace-style curvature extraction via sparse Hessian and Cholesky yields efficient marginal uncertainty for safety-relevant outputs.

between mass flow and volumetric return. Rather than attempt to model detailed composition, the estimator treats swelling as a bounded function of a normalized dissolved fraction $\chi_d t = M_d t M_l t$, where $M_l t$ is an effective liquid mass that is slowly varying over the horizon (10). The swelling factor $B_l \chi_d, p, T$ is represented by a smooth bounded parametric form whose parameters are treated as uncertain. This representation allows the estimator to attribute observed pit gain to swelling when consistent with other signals, without forcing swelling to explain patterns that are more consistent with free gas or with instrument bias.

The dynamics couple pressure, flow, and inventories. Pressure evolution is governed by compressible storage and by balance between inlet and outlet boundary conditions, hydrostatic gradients, and friction. A low-order dynamics can be expressed as a network-like model where each pressure node has a storage coefficient and each segment has a resistive element. The resistive elements depend on friction parameters and on mixture density and viscosity (11). The mixture density depends on free-gas proxy and on swollen liquid density. This yields a nonlinear but smooth dynamics for pt and qt that can reproduce the dominant transient shapes induced by choke actuation and pump ramps.

The inventory dynamics represent influx, migration, and dissolution exchange at the coarse level. Influx is represented as an uncertain source $M_{in} t$ parameterized by onset time and magnitude, with a low-dimensional shape to preserve identifiability. Free gas outflow is represented by a function of near-surface free-gas proxy and flow. Dissolution exchange is represented as relaxation toward equilibrium, with equilibrium dissolved inventory depending on pressure and temperature proxies. The equilibrium map is treated as bounded and monotone in pressure, reflecting the tendency for higher pressure to increase solubility in relevant regimes (12). The kinetic rate is treated as uncertain within plausible bounds and is estimated only when data supports it.

The measurement model maps the latent state to observed surface signals. Surface casing pressure is linked to the top pressure node. Standpipe pressure is linked to friction and flow at the inlet. Flow-in and flow-out are linked to qt, with flow-out also influenced by compressible storage and by swelling-modified volumetric return. Pit volume is linked to the time integral of flow imbalance and to swelling effects because swelling changes the volumetric return for a given mass return (13). Pit measurement is subject to bias and drift, modeled explicitly as a bias state with slow dynamics. Similarly, flow meters may have multiplicative scale factors, also represented as uncertain or slowly varying.

A key choice is to model measurement noise as temporally correlated rather than independent. Surface signals in drilling are filtered and often display colored noise due to pump pulsations, choke oscillations, and sensor filtering. If the estimator assumes independent noise, it will overcount information and yield overconfident posteriors. The factor-graph formulation allows correlated noise to be modeled by augmenting the state with noise processes or by introducing factors that connect consecutive measurement residuals (14). Bias drift is represented explicitly, and short-term colored noise is represented by low-order autoregressive residual factors.

Uncertainty in closure parameters is represented by uncer-

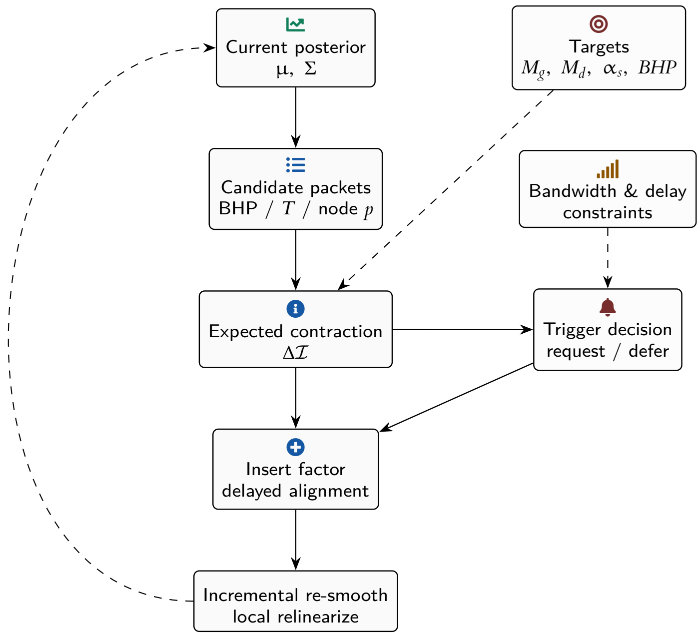

Figure 4. Event-triggered telemetry scheduling on the factor graph. The smoother exposes a posterior covariance structure that supports lightweight estimates of expected uncertainty contraction for safety-relevant targets. Candidate measurement packets are evaluated under bandwidth and delay constraints, triggering selective requests whose factors are inserted at their physical timestamps for consistent retrospective smoothing.

tain parameters θ that enter friction, compressibility storage, swelling response, and equilibrium dissolution maps. Because the estimator operates under partial observability, not all closure parameters are identifiable, and attempting to estimate them all can degrade performance. The framework therefore partitions parameters into an estimated subset and a nuisance subset. The estimated subset includes the most influential bias terms and one or two dominant friction multipliers, while the nuisance subset is represented by prior uncertainty that is propagated into posterior uncertainty of outputs. This prevents the smoother from absorbing all mismatch into influx or dissolution states (15).

The reduced state representation is not claimed to be unique. Its purpose is to provide a basis for sparse inference that can encode thermodynamic consistency and yield robust estimates under intermittent telemetry. The next section introduces the factor graph that encodes dynamics, measurements, thermodynamic constraints, and bounds in a unified probabilistic model.

3. Factor-Graph Formulation with Inequality-Constrained Thermodynamic Factors

A factor graph represents a joint distribution over variables as a product of factors, each factor encoding a probabilistic relationship among a subset of variables. For smoothing, variables correspond to states at each time step, parameters, and bias states, while factors correspond to dynamics, measurements, priors, and constraints. The appeal of this representation is twofold: it makes asynchronous sensor fusion natural, and it exposes sparsity that can be exploited for efficient optimization (16).

Let x_k denote the latent state at time t_k, containing pressure nodes, flow proxy, inventories, and near-surface gas proxy. Let β_k denote bias states, such as pit bias and flow scale drift. Let θ denote static or slowly varying parameters. The complete variable set over a horizon of N steps is $X = \{x_0, \dots, x_N, \beta_0, \dots, \beta_N, \theta\}$. Measurements at time k are denoted y_k, with potentially missing components due to sensor outages and with asynchronous timestamps handled by inserting measurement nodes at the appropriate times.

The joint posterior is

$$pX \mid Y \propto px_0\, p\beta_0\, p\theta \,{}_{k=0}^{N-1}\, px_{k1} \mid x_k, \theta \,{}_{k=0}^{N-1}\, p\beta_{k1} \mid \beta_k \,{}_{k\in\mathcal{K}}\, py_k \mid x_k, \beta_k, \theta \tag{3.1}$$

where $\mathcal{K}$ indexes times with measurements. This factorization already yields sparsity because each dynamics factor links only consecutive states, and each measurement factor links only the current state and bias (17). Thermodynamic and bound constraints are introduced as additional factors that link components within a state and parameters across time.

The dynamics factor $px_{k1} \mid x_k, \theta$ is derived from the reduced dynamics with additive noise representing unmodeled disturbances and model reduction error. The covariance of this noise is not assumed constant; it depends on operating conditions, reflecting that model mismatch can be larger during aggressive actuation or near phase appearance. This dependence is encoded by allowing the process noise covariance to be a function of x_k and u_k, with conservative bounds. The factor is implemented as a Gaussian or robust Gaussian in the residual $x_{k1} - f x_k, u_k; \theta$.

Measurement factors map the state to observed signals.

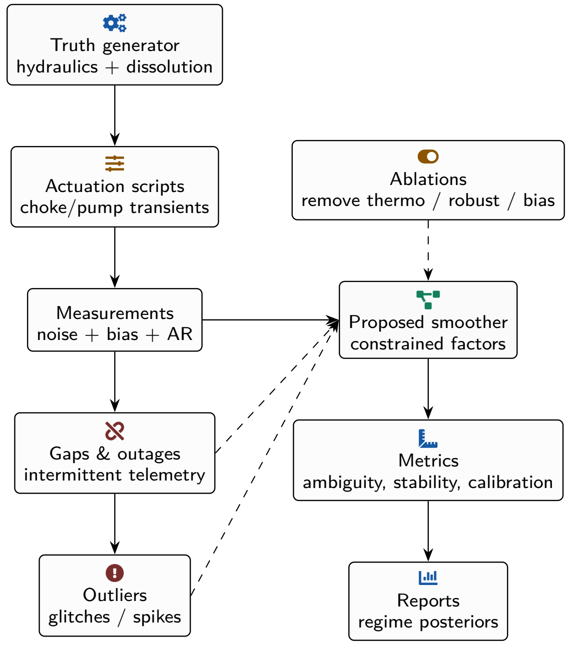

Figure 5. Numerical experiment workflow for intermittent telemetry and swelling ambiguity. A synthetic truth model produces surface and downhole measurement streams under structured actuation, then injects telemetry gaps, correlated noise, bias drift, and outliers. The proposed constrained smoother is evaluated with targeted ablations, and performance is summarized by regime-separation behavior, stability under long gaps, and uncertainty calibration diagnostics.

Because measurements can include outliers, robust likelihoods are used, implemented by heavy-tailed residual models or by scale-mixture representations. The factor-graph structure permits this without losing sparsity by introducing latent scale variables per measurement residual (18). Bias states enter additively or multiplicatively as appropriate.

Thermodynamic consistency is encoded by factors that relate dissolved inventory, pressure, and swelling. The core relationship is that dissolved fraction tends toward an equilibrium map that is monotone in pressure and temperature, and swelling is a bounded function of dissolved fraction and state. In the factor graph, equilibrium is not enforced as an equality at each time, because kinetics can be slow. Instead, a relaxation residual is used,

$$r_{d,k} = \chi_{d,k1} - \chi_{d,k} - \Delta t\, \kappa_d \big(\chi_d^{\star} p_k, T_k - \chi_{d,k}\big) \tag{3.2}$$

with a factor penalizing $r_{d,k}$ according to uncertainty in kinetics and in the equilibrium map. The equilibrium map itself is represented by a bounded parametric function, and its uncertainty is encoded by a prior on its parameters (19). The factor is designed to be smooth, enabling efficient optimization.

Inequality constraints are crucial because key variables are bounded: dissolved fraction lies in $0, 1$, free-gas proxy lies in $0, 1$, densities are positive, and swelling factor is at least 1. Hard constraints can be enforced by constrained optimization, but that can be computationally burdensome in large smoothing problems. The framework therefore uses barrier-like factors that encode bounds probabilistically, avoiding hard projection. For example, a sigmoid reparameterization is used for fractions, representing $\chi_d = \sigma\eta_d$ and $\alpha_s = \sigma\eta_s$ for unconstrained variables η_d, η_s. This ensures bounds by construction while keeping factors smooth (20). For positivity constraints such as density, logarithmic reparameterization is used. These transformations are internal to the factor definitions and do not change the factor-graph sparsity.

The swelling factor is linked to dissolved fraction via a bounded parametric form. A representative relation is

$$B_{l,k} = 1 \;\; b_1\, \chi_{d,k} \;\; b_2\, \chi_{d,k}^2 \tag{3.3}$$

with constraints that keep $B_{l,k} \geq 1$ across the range. The coefficients b_1, b_2 are included in θ with priors and bounds. Because swelling affects the mapping between mass and volume, it enters measurement factors for pit and flow-out (21). This creates a pathway by which pit signals can inform χ_d, but only in combination with pressure and flow signals, which reduces the risk that pit bias alone drives swelling estimates.

A key design objective is to separate explanations: bias drift should be captured by bias variables, friction variability by friction parameters, and dissolution by dissolved inventory variables. Factor graphs support this separation by allowing explicit priors and smoothness constraints on each variable class. Bias variables have strong smoothness priors that represent slow drift; friction multipliers have priors centered at nominal with moderate variance; dissolved fraction dynamics have priors shaped by kinetic uncertainty; and influx parameters have priors reflecting plausibility and can be activated only when evidence accumulates. The result is that the posterior tends to assign deviations to the variable class that can explain them with the least violation of priors, but because the factor graph is coupled, this assignment is informed by multi-sensor consistency rather than by single-channel residuals.

Table 2. Reduced annular hydraulics components that define the state space for inference under managed pressure drilling.

Component	Representation	Captures	Notes
Pressure field	Node vector pt	Hydrostatic structure and major friction segments	Coarse depth grid, tuned to well geometry
Flow	Scalar proxy qt	Net volumetric through-flow	Linked to standpipe, return-flow, pit signals
Compressible storage	Lumped storage coefficients	Dynamic response to boundary actuation	Encodes effective compliance of wellbore and fluids
Free-gas inventory	$M_g t$ and $\alpha_s t$	Holdup and surface-handling risk	Sensitive to compressibility-driven signatures
Dissolved inventory	$M_d t$ and $\chi_d t$	Dissolution buffering and swelling effects	Linked to pressure and temperature proxies
Swelling factor	$B_l \chi_d, p, T$	Density / specific-volume modification	Smooth bounded parametric map with uncertainty

The maximum a posteriori estimate corresponds to minimizing the negative log posterior, yielding a sparse nonlinear optimization (22). Writing residuals $r_i X$ for each factor and associated covariance or scale, the objective is

$$\min_{X} \sum_{i} \frac{1}{2} \|r_i X\|^2_{W_i} \qquad \text{robust penalties} \tag{3.4}$$

with W_i the inverse covariance weights. The sparsity pattern in the Jacobian reflects the local factor connections, yielding a banded or block-sparse structure that can be exploited by sparse linear algebra in Gauss–Newton or Levenberg–Marquardt iterations.

To incorporate intermittent telemetry, downhole measurements are inserted as factors at their arrival times. Because the graph is a smoother, delayed measurements can be inserted retrospectively, and the estimate can be updated by relinearization in a sliding window. This is operationally valuable because telemetry can arrive late (23). The incremental update is efficient because only a local part of the graph needs to be updated, and sparsity ensures that complexity scales near-linearly in window length for fixed state dimension.

The factor-graph formulation provides a structured optimization, but stable and calibrated inference also requires uncertainty quantification, not only point estimates. The next section derives a hybrid inference strategy that combines constrained variational approximations with Laplace corrections to produce bounded, interpretable posterior uncertainty under inequality constraints and robust residual models.

4. Hybrid Variational–Laplace Inference with Bound-Preserving Posteriors

While maximum a posteriori estimates are useful for tracking, safety decisioning requires uncertainty quantification, particularly under intermittent telemetry where ambiguity can persist. In factor graphs with Gaussian factors, one can approximate the posterior as Gaussian around the MAP estimate using the Laplace approximation. However, in the present setting, robust likelihoods, inequality constraints, and nonlinear thermodynamic factors produce non-Gaussian posteriors that can be poorly approximated by a single Gaussian (24). At the same time, fully nonparametric inference can be too expensive for real time. The framework therefore adopts a hybrid strategy: a structured variational approximation captures non-Gaussian features and respects bounds, while a Laplace correction around the variational mode provides local curvature information for fast uncertainty propagation.

The variational approximation chooses a family qX and minimizes $\mathrm{KL}q\|p$ subject to tractability. A common choice is a mean-field factorization, but mean-field can be too crude because strong correlations exist between pressure, flow, and friction, and between dissolved fraction and pit bias. The chosen variational family therefore uses a sparse Gaussian graphical model in transformed coordinates, preserving correlations along the time chain and among a subset of strongly coupled variables. In effect, q is defined by a sparse precision matrix whose sparsity follows the factor graph but with selected fill-in to capture key couplings. This yields an approximation that remains computationally manageable while avoiding the worst underconfidence typical of mean-field (25).

Bound constraints are handled by reparameterization. For bounded variables such as dissolved fraction and near-surface gas proxy, unconstrained variables are used in the variational family, and the physical variables are obtained by smooth transforms. The variational distribution is defined in the unconstrained space, which is Gaussian, and the induced distribution in physical space is non-Gaussian but bounded. This yields physically admissible uncertainty intervals without clipping, which is critical because clipping can systematically distort tail

Table 3. Schematic structure of the augmented state at time k, combining hydraulics, thermodynamic partitioning, bias, and uncertainty processes.

Block	Variables at step k	Dimension	Role in diagnosis
Core hydraulics	p_k, q_k	n_p 1	Encodes pressure distribution and flow transients
Gas inventories	$M_{g,k}$, $M_{d,k}$, $\alpha_{s,k}$, $\chi_{d,k}$	3–4	Partitioned gas mass and near-surface risk proxy
Bias states	Pit bias, flow scale, pressure offsets	2–5	Represent drift and calibration errors in sensors
Closure parameters	Friction multipliers, swelling coefficients, kinetics	3–8	Capture dominant model mismatch directions
Noise processes	Colored-noise states, scale variables	3–6	Model temporal correlation and outlier robustness

probabilities and bias risk metrics.

Robust measurement factors are handled by introducing latent scale variables. For example, a Student-t likelihood can be represented as a Gaussian residual with an inverse-gamma scale (26). In the variational approximation, these scale variables can be integrated out approximately or maintained explicitly with conjugate updates. Maintaining them explicitly allows the posterior to downweight outliers in a data-driven way, reducing the tendency of the estimator to explain glitches by implausible state changes. The factor graph remains sparse because each scale variable connects only to a single residual.

The variational update can be performed by coordinate ascent in blocks that correspond to time slices or variable groups, using linearization for nonlinear factors. Because the dynamics factors connect consecutive time slices, message passing interpretations emerge. However, because of nonlinearity and robust factors, exact message passing is intractable (27). The framework uses iterative linearization and sparse solves, analogous to iterated extended Kalman smoothing but with variational reweighting and bound-preserving transforms. This yields stable behavior under long telemetry gaps because the dynamics factors propagate uncertainty forward, while measurement factors contract it when data arrives.

After variational convergence, a Laplace correction is applied locally. The idea is to compute the Hessian of the negative log posterior at the variational mean and to use it to extract a local Gaussian approximation for selected marginals, particularly those needed for downstream decisioning such as bottomhole pressure, surface gas proxy, and inventories. This correction is efficient because the Hessian inherits sparsity from the factor graph. Sparse Cholesky factorization yields marginal variances and selected covariances without full inversion (28). The correction also provides a diagnostic of identifiability: directions in which the Hessian is ill-conditioned correspond to unidentifiable combinations of influx, dissolution, and friction.

A crucial aspect is to avoid overconfidence due to model mismatch. Even with robust likelihoods, the posterior can become overly tight if process noise is underestimated. The framework therefore incorporates adaptive covariance inflation based on innovation statistics. When measurement residuals remain systematically large relative to their modeled uncertainty, process noise is increased locally, which expands posterior uncertainty and prevents the estimator from forcing unrealistic state trajectories. This inflation is not arbitrary; it is guided by a consistency criterion that compares predicted and observed residual covariance over a window (29).

The hybrid inference produces posterior distributions for latent variables and parameters. These posteriors can be used directly to compute risk measures such as probabilities of constraint violation. However, because the focus of this paper is the estimation architecture rather than risk quantification per se, the downstream use is framed as regime discrimination and telemetry scheduling. Regime discrimination is performed by examining posterior mass in the free-gas and dissolved-gas inventories and by examining posterior correlations between pit signals and dissolved fraction. When dissolved fraction posterior increases while free-gas posterior remains bounded and pressure signals remain consistent, the event is interpreted as swelling-consistent. When free-gas posterior increases and compressibility-sensitive residuals dominate, the event is interpreted as free-gas-consistent (30). This interpretation is not a hard classification; it is a posterior diagnostic that can inform operational response.

Telemetry scheduling is motivated by the observation that uncertainty contraction is limited by information content. Under intermittent telemetry, the estimator may remain ambiguous. If a downhole telemetry packet is available but bandwidth-limited, it is valuable to request the measurement when it will maximally reduce uncertainty about critical latent variables. Because the factor-graph inference yields a posterior covariance structure, it can support an information gain calculation that drives an event-triggered telemetry policy. This is developed in the next

Table 4. Representative factor types in the factor-graph formulation and their coupling to latent variables and parameters.

Factor type	Symbolic form	Neighboring variables	Primary purpose
Prior	$px_0,\ p\theta$	$x_0,\ \theta$	Initialize trajectory and closure uncertainty
Dynamics	$px_{k1} \mid x_k, \theta$	$x_k,\ x_{k1},\ \theta$	Propagate state under reduced hydraulics model
Bias evolution	$p\beta_{k1} \mid \beta_k$	$\beta_k,\ \beta_{k1}$	Impose slow drift on sensor biases
Measurement	$py_k \mid x_k, \beta_k, \theta$	$x_k,\ \beta_k,\ \theta$	Link latent state to surface and downhole signals
Thermodynamic relaxation	$p\chi_{d,k1} \mid \chi_{d,k}, p_k, T_k$	$\chi_{d,k},\ \chi_{d,k1},\ p_k$	Encode pressure-dependent dissolution kinetics
Bound / reparameterization	Implicit transforms	Fractions, densities, B_l	Enforce positivity and unit-interval constraints

section (31).

5. Event-Triggered Telemetry and Measurement Scheduling via Expected Posterior Contraction

Downhole telemetry is often bandwidth constrained and can be intermittent due to tool limitations, formation properties, or operational choices. Even when telemetry is available, transmitting every measurement at full rate may be infeasible. A digital twin that explicitly models latent dissolution and swelling states benefits strongly from downhole pressure or temperature telemetry, yet such telemetry may be sparse. This motivates a scheduling problem: when should telemetry be requested or prioritized, and which measurement should be sent, to maximally reduce uncertainty about safety-relevant quantities?

The proposed approach treats telemetry scheduling as a decision problem on the factor graph. At each time step, the estimator has a posterior distribution over the current state and parameters, represented by a variational distribution and local curvature (32). A candidate telemetry measurement corresponds to adding a prospective factor to the graph. The expected reduction in uncertainty from adding that factor can be approximated using linearized information measures. The scheduling policy chooses to request telemetry when the expected benefit exceeds a threshold, subject to bandwidth and operational constraints.

Let z denote a candidate measurement type, such as bottomhole pressure, an intermediate pressure node, or a temperature proxy. The expected information gain can be approximated by the reduction in entropy of a target subset of variables, such as free-gas inventory and near-surface gas proxy. Under a local Gaussian approximation, entropy is a function of covariance (33). The reduction in entropy from adding a linear measurement factor can be computed analytically from prior covariance and measurement noise covariance. In the nonlinear setting, a linearization around the current posterior mean is used. The resulting information gain estimate is

$$\Delta\mathcal{I}z \approx \frac{1}{2}\log\frac{\det\Sigma_{\text{prior}}}{\det\Sigma_{\text{post}}z} \tag{5.1}$$

for the target subspace, where $\Sigma_{\text{post}}z$ is the posterior covariance after incorporating the prospective measurement. This computation can be performed efficiently using Schur complements and sparse linear algebra because only a small subset of variables is targeted.

A practical scheduling policy must also account for the fact that telemetry arrives with delay and may be unreliable. The factor-graph representation accommodates delay by inserting the measurement factor at the time the measurement corresponds to, even if it arrives later (34). The scheduling decision is then not purely immediate; it is a decision about expected future contraction given that measurement will be available. The estimator maintains a short-horizon prediction of how uncertainty will evolve under dynamics factors, and it evaluates information gain relative to that predicted uncertainty. This encourages requesting telemetry when the estimator expects ambiguity to grow, such as during aggressive actuation or suspected influx onset.

The policy is also conditioned on risk relevance. If the posterior suggests a high probability of approaching a pressure window or surface handling constraint, telemetry that reduces uncertainty in bottomhole pressure or gas inventory is prioritized. If the posterior suggests a stable nominal regime, telemetry can be deferred (35). This prioritization is implemented by weighting the target subspace and by including a risk proxy, such as the posterior probability that bottomhole pressure will exceed a bound within a short horizon. The scheduling

Table 5. Qualitative comparison between swelling-buffered and free-gas-dominated influx regimes in terms of surface signatures and latent posterior structure.

Diagnostic feature	Swelling-buffered kick	Free-gas-dominated kick	Posterior-based distinction
Early pit response	Persistent pit gain with modest pressure distortion	Pit gain often co-occurs with strong compressibility effects	Pit gain correlated with χ_d vs. M_g and α_s
Surface gas indicators	Weak or delayed surface gas signatures	Rapid growth of near-surface gas proxy	Posterior mass shifts in α_s for free-gas case
Pressure–flow coupling	Changes consistent with density / swelling	Pronounced compressibility-driven transients	Geometry of pressure–flow residuals in latent space
Telemetry value	High value for downhole pressure to pin solubility	Useful but often nonessential early	Difference in expected information gain for pressure packets
Operational implication	Early pit gain with limited near-term surface load	Stronger emphasis on surface handling and venting	Regime-tagging based on joint inventory posteriors

objective becomes a weighted information gain, reflecting both uncertainty reduction and risk relevance.

Because the system is nonlinear and uncertainty can be non-Gaussian, the linearized information gain is an approximation. The framework therefore uses a conservative scheduling approach: it requests telemetry only when the estimated gain is substantially above the threshold, and it uses posterior diagnostics to avoid oscillatory requesting. Additionally, the robust likelihood framework can downweight telemetry outliers if the telemetry packet is corrupted. This is important because downhole telemetry can be noisy (36).

An event-triggered policy can be implemented without full optimization. A simple policy is to request telemetry when the predicted variance of a critical latent variable exceeds a threshold, or when the correlation between pit gain and dissolved fraction becomes highly uncertain. However, the factor-graph approach enables more targeted policies that account for which measurement type reduces which uncertainty direction. For example, downhole pressure may reduce friction-dissolution ambiguity, while downhole temperature may reduce equilibrium dissolution ambiguity. The policy can therefore adapt to the current posterior structure.

This scheduling layer is designed to be modular (37). It does not require modification of the underlying estimator; it uses the estimator's covariance and Jacobian information. In deployment, the policy could interface with existing telemetry systems by issuing requests or by selecting among available packet types. The decision logic can also incorporate operational constraints, such as not requesting additional telemetry during known tool transitions.

Telemetry scheduling closes a loop between estimation and sensing: the estimator guides which data to obtain, and the obtained data contracts the posterior. This loop is particularly valuable in dissolution-buffered regimes where early surface signals are ambiguous. In such regimes, a small number of well-chosen downhole measurements can sharply reduce ambiguity between swelling and free gas, enabling more appropriate operational response (38). The next section evaluates the combined estimation and scheduling framework in numerical experiments designed to stress intermittent telemetry, actuation transients, and closure uncertainty.

6. Numerical Experiments under Intermittent Telemetry, Closure Uncertainty, and Swelling Ambiguity

The numerical experiments evaluate the proposed factor-graph smoothing framework on scenarios designed to reflect the operational challenges that motivate the method. The emphasis is not on matching a specific field dataset, but on demonstrating stability, interpretability, and uncertainty behavior under realistic confounds. A synthetic truth model generates measurement streams, including surface pressures, flow rates, pit volume, and optional intermittent downhole telemetry. The truth model includes compressibility, friction, dissolution exchange, and swelling, with parameters selected from plausible ranges. The estimator uses the reduced model and represents closure uncertainty through priors and process noise, creating a controlled mismatch setting (39).

The first experiment is a nominal managed pressure operation with frequent choke actuation and pump ramps but no influx. This experiment tests whether the smoother can track baseline transients without attributing them to spurious gas inventory changes. The factor graph includes bias states for pit and flow scaling, and robust residual factors to handle occasional glitches. Under this setting, the posterior over free-

Table 6. Major sources of uncertainty in the drilling environment and how they are represented within the smoothing framework.

Uncertainty class	Representative sources	Probabilistic representation	Effect on inference
Fluid properties	Gas density, viscosity, compressibility	Priors on closure parameters; nuisance uncertainty	Influences hydrostatic gradients and friction losses
Thermodynamic closure	Solubility curve, swelling response	Bounded parametric maps with priors	Controls trade-off between dissolved and free gas
Sensor bias and drift	Pit offset, flow scale, pressure zero	Bias states with smooth evolution	Separates instrumentation effects from physical changes
Colored noise	Pump pulsations, choke oscillations	Low-order noise processes, AR residuals	Prevents overconfident fits to filtered signals
Model reduction error	Coarse spatial and temporal summaries	State-dependent process noise	Limits spurious structure in under-resolved dynamics
Outliers	Telemetry glitches, transient dropouts	Heavy-tailed likelihood via scale mixtures	Downweights anomalous residuals without clipping states

gas and dissolved-gas inventories remains concentrated near nominal, while the posterior over friction multipliers and bias states adapts slowly within bounds. The uncertainty grows modestly during aggressive actuation and contracts when steady periods provide consistent measurements. Telemetry scheduling remains mostly inactive because expected information gain is low and risk proxies remain low (40).

The second experiment introduces a swelling-buffered influx at depth. The influx is small and occurs under high pressure, leading to significant dissolution. Pit gain is observed, but surface gas proxies remain low in the early window. The challenge is that pit gain can be explained by swelling, by bias drift, or by small free gas. The factor graph's explicit bias state prevents pit drift from being forced into swelling, and pressure and flow measurements constrain the feasible explanations. The posterior indicates increased dissolved inventory with bounded free-gas inventory, and the posterior correlation between dissolved inventory and pit gain becomes strong (41). Under intermittent telemetry gaps, uncertainty increases, but the estimator remains stable and does not produce unphysical excursions because bounds are enforced by reparameterization. When a downhole pressure telemetry packet is injected, the posterior contracts sharply, and the telemetry scheduler, when enabled, requests such a packet early because expected information gain is high due to friction-dissolution ambiguity.

The third experiment introduces a free-gas-dominated influx with weaker dissolution. Here, surface pressure and flow-out signals exhibit stronger compressibility-consistent deviations. The posterior over free-gas inventory increases, and the near-surface gas proxy distribution shifts upward earlier than in the swelling-buffered case. The estimator differentiates the regimes not by a single signal but by the joint posterior: in this case, pit gain aligns with increased free-gas proxy and with pressure-flow coupling changes (42). Telemetry scheduling still requests downhole pressure, but its information gain is now moderate because surface signals already contain substantial information about free-gas dominance. The scheduler therefore triggers less frequently, illustrating that telemetry requests are adaptive to regime identifiability.

The fourth experiment examines closure uncertainty and bias confounding. Gas property scaling parameters are perturbed in the truth model, and the estimator represents them as nuisance uncertainty rather than as estimated parameters. This causes the estimator to inflate uncertainty in pressure predictions, particularly in the bottomhole pressure proxy. The posterior for free and dissolved inventories remains meaningful but has broader credible intervals (43). Because the estimator is not overconfident, it avoids attributing pressure mismatch to a large influx. The telemetry scheduler becomes more active because downhole pressure telemetry reduces property-induced ambiguity in pressure distribution. This illustrates a practical benefit: when closure uncertainty dominates, additional measurements can be more valuable than tighter priors.

The fifth experiment focuses on long telemetry gaps. Downhole telemetry is removed for extended intervals, and surface signals are partially missing due to sensor outages. The factor graph naturally accommodates missing data by omitting factors, and the smoother propagates uncertainty through dynamics factors (44). The posterior uncertainty grows, but the MAP trajectory remains stable. When telemetry resumes, delayed packets are inserted retroactively, and the smoother updates the past window efficiently. This retroactive update is important

Table 7. Example downhole telemetry channels considered in the event-triggered measurement scheduling layer.

Telemetry channel	Typical content	Latent variables most informed	Scheduling heuristic
Bottomhole pressure	Local annular pressure at depth	p_k profile, dissolution equilibrium	Request when friction–dissolution ambiguity is high
Intermediate annular pressure	Pressure at intermediate tool	Pressure gradient, friction multipliers	Prioritize during large choke or pump changes
Downhole temperature proxy	Coarse temperature at depth	Solubility curve, equilibrium $\chi_d^\star$	Use when swelling-driven pit gain is suspected
Downhole flow proxy	Approximate local flow rate	Storage vs. friction separation	Trigger when surface flow readings are inconsistent
Tool health / QC flags	Packet quality indicators	Robustness scales, noise models	Adjust likelihood scale; no direct state update

because it prevents the estimator from being permanently biased by a gap; the estimator can correct its understanding when data arrives later, which is common in drilling telemetry.

The sixth experiment evaluates the effect of robust likelihoods. Outliers are injected into flow-out measurements to represent transient sensor glitches. Without robust factors, the smoother attempts to explain the glitch by abrupt state changes, which can create spurious gas inventory estimates (45). With scale-mixture robust factors, the outlier is downweighted, and the posterior remains consistent. This reduces false alarms and improves the stability of downstream telemetry scheduling, because the scheduler does not interpret an outlier as a sudden increase in uncertainty requiring immediate telemetry.

The seventh experiment evaluates ablations in thermodynamic constraint representation. When dissolution exchange factors are removed and swelling is not represented, the estimator can still fit pressure and flow signals by adjusting friction and by interpreting pit gain as free gas or bias. However, the posterior becomes less interpretable and can overpredict near-surface gas proxy in swelling-buffered scenarios. When bounded swelling factors are included but not tied to dissolved inventory by thermodynamic factors, the estimator can fit pit gain by swelling but lacks a constraint linking swelling to pressure, leading to inconsistent behavior under pressure modulation (46). The thermodynamic factors prevent such inconsistency by encoding that swelling behavior is coupled to pressure-dependent solubility trends.

Across experiments, computational performance is assessed qualitatively by noting that the factor graph exploits sparse structure. With a fixed window length and moderate state dimension, Gauss–Newton iterations with sparse linear solves remain feasible in real time. The hybrid variational–Laplace approach adds overhead but yields improved calibration and stability under heavy-tailed noise. Telemetry scheduling computations are lightweight because they operate on low-dimensional Schur complements of the covariance.

These experiments emphasize that the framework is not designed to replace operational judgment or well-control procedures (47). It is designed to provide a stable, uncertainty-aware estimate of latent inventories and a principled mechanism to decide when additional telemetry is valuable. It also provides diagnostics that can separate swelling-consistent patterns from free-gas-consistent patterns in a way that naturally accounts for bias and closure uncertainty.

7. Conclusion

This paper developed a factor-graph smoothing framework for real-time kick diagnosis under managed pressure drilling when dissolution and swelling can buffer free gas and alter early surface signatures. The approach introduced a reduced but physically anchored state representation with explicit partitioning between free and dissolved gas inventories and swelling-modified volumetric mapping, enabling pit-volume trends to be interpreted in a thermodynamics-consistent latent-variable model rather than in a free-gas-only heuristic. The joint posterior was encoded in a sparse factor graph that accommodates intermittent telemetry and asynchronous sensors, with inequality constraints enforced by bound-preserving reparameterization and robust likelihoods implemented through scale-mixture factors. A hybrid variational–Laplace inference scheme was derived to produce physically admissible posteriors and calibrated uncertainty without nonphysical clipping, and an event-triggered telemetry policy was co-designed to request downhole measurements when expected posterior contraction for safety-relevant latent variables is largest (48).

The framework was motivated by the operational reality that early-stage ambiguity is an observability problem compounded by thermodynamic partitioning and closure uncertainty. Manikonda et al. (2021) (49) developed a thermodynamic swelling modeling approach for drilling mud under kick conditions that clarified how dissolved gas can induce volumetric expansion in a mechanistically interpretable manner, and the present work used that conceptual structure to justify bounded thermodynamic factors that constrain swelling behavior without relying on a full equation-of-state solver online. Numerical experiments demonstrated stable inference under aggressive actuation, long telemetry gaps, bias drift, and closure mismatch, with the estimator providing regime-sensitive posterior diagnostics that separate swelling-consistent pit gain from free-gas-dominated compressibility signatures.

Limitations include dependence on a reduced dynamics model that may omit regime-dependent slip phenomena and on uncertainty envelopes that must be calibrated conservatively to avoid underconfidence. Future work can incorporate richer temperature coupling, extend the factor graph to include additional downhole sensors when available, and integrate the posterior outputs into risk-aware control or certification layers. Within the present scope, factor-graph smoothing with thermodynamics-consistent latent states provides a tractable route to dissolution-aware diagnosis that remains stable under intermittent telemetry and operational transients (50).

References

[1] S. Ray and S. D. S. Sinha, "Non-equilibrium dynamics of quantum many body systems: Application to ultracold atomic gases," 5 2019.

[2] O. L. A. Santos, "Well-control operations in horizontal wells," *SPE Drilling Engineering*, vol. 6, pp. 111–117, 6 1991.

[3] L. Rocha and A. Bourgoyne, "A new simple method to estimate fracture pressure gradient (includes associated paper 37685)," *SPE Drilling & Completion*, vol. 11, pp. 153–159, 9 1996.

[4] K. Manikonda, A. R. Hasan, O. Kaldirim, N. Rahmani, and M. A. Rahman, "Estimating swelling in oil-based mud due to gas kick dissolution," in *International conference on offshore mechanics and arctic engineering*, vol. 84430, p. V011T11A039, American Society of Mechanical Engineers, 2020.

[5] B. Patel, T. D. Cooper, and W. Billings, "The application of advanced gas extraction and analysis system complements early kick detection & control capabilities of managed pressure drilling system with added hse value," *SPE/IADC Drilling Conference*, 3 2013.

[6] A. K. Sleiti, W. A. Al-Ammari, M. Abdelrazeq, M. El-Naas, M. A. Rahman, A. Barooah, R. Hasan, and K. Manikonda, "Comprehensive assessment and evaluation of correlations for gas-oil ratio, oil formation volume factor, gas viscosity, and gas density utilized in gas kick detection," *Journal of Petroleum Science and Engineering*, vol. 207, p. 109135, 2021.

[7] N. Taryana, "Perhitungan kecepatan gelombang akustik refleksi dalam analisa performansi sumur minyak menggunakan well analyzer echometer berbasis total well management (twm)," 11 2016.

[8] Z. Wang and B. Sun, "Deepwater gas kick simulation with consideration of the gas hydrate phase transition," *Journal of Hydrodynamics*, vol. 26, pp. 94–103, 2 2014.

[9] S. Stokka, E. Cayeux, D. Gardner, S. Kragset, H. P. Lohne, E. Randeberg, H. J. Skadsem, B. Aas, H. Kyllingstad, T. Larsen, and A. Saasen, "Long reach well concept," *IADC/SPE Drilling Conference and Exhibition*, 3 2016.

[10] D. Whitman, J. Evers, and R. Terry, "Using computer graphics and animation to teach petroleum engineering concepts," in *International Meeting on Petroleum Engineering*, SPE, 3 1992.

[11] M. Runtuwene, S. Suprihono, D. Rizka, A. E. Prasetia, J. S. S. Toralde, and S. W. Nas, "Pressurized mud cap drilling drastically reduces non-productive time in soka field, south sumatera," in *Middle East Drilling Technology Conference & Exhibition*, SPE, 10 2009.

[12] H. J. Dervo and B. Blom-Jensen, "Comparison of quantitative blowout risk assessment approaches," in *SPE International Conference on Health, Safety, and Environment in Oil and Gas Exploration and Production*, SPE, 3 2004.

[13] R. Samuel, T. W. Engler, and S. Z. Miska, "A practical technique to estimate the formation thickness of a kicking zone," *Journal of Energy Resources Technology*, vol. 124, pp. 1–7, 3 2002.

[14] W. M. F. W. Hassan, T. Thamilyanan, A. A. Suggust, M. Z. Usop, N. Hamdan, A. M. Razali, N. Latif, H. Bakar, and S. Kumar, "The challenges and lessons learned from the unanticipated long run well unloading campaign in t field, malaysia," in *SPE/IATMI Asia Pacific Oil & Gas Conference and Exhibition*, SPE, 10 2021.

[15] A. Ayala, D. M. Paret, A. P. Martínez, G. Piccinelli, A. Sánchez, and J. S. R. Montaño, "Kicks of magnetized strange quark stars induced by anisotropic emission of neutrinos," *Physical Review D*, vol. 97, pp. 103008–, 5 2018.

[16] Z. Lippai, Z. Frei, and Z. Haiman, "Prompt shocks in the gas disk around a recoiling supermassive black hole binary," *The Astrophysical Journal*, vol. 676, pp. L5–L8, 3 2008.

[17] J. Floß, A. Kamalov, I. S. Averbukh, and P. H. Bucksbaum, "Observation of bloch oscillations in molecular rotation," *Physical review letters*, vol. 115, pp. 203002–203002, 11 2015.

[18] E. M. Rossi, G. Lodato, P. J. Armitage, J. E. Pringle, and A. J. King, "Black hole mergers: the first light," *Monthly Notices of the Royal Astronomical Society*, vol. 401, pp. 2021–2035, 1 2010.

[19] T. Nuralishahi, M. Vahmani, E. D. Putra, M. H. Wun, K. K. Thakur, P. W. Aung, C. Coman, S. Delfani, K. Wimbridge, N. Rodriguez, and J. Samaan, "Optimising horizontal coal seam gas wells by combining reservoir simulation and transient well modelling," in *SPE Asia Pacific Oil and Gas Conference and Exhibition*, SPE, 10 2018.

[20] E. Nakagawa and A. C. Lage, "Kick and blowout control developments for deepwater operations," *IADC/SPE Drilling Conference*, 2 1994.

[21] H. Zhou, H. Fan, H. Wang, X. Niu, and G. Wang, "A novel multiphase hydrodynamic model for kick control in real time while managed pressure drilling," in *SPE/IADC Middle East Drilling Technology Conference and Exhibition*, SPE, 1 2018.

[22] R. Rommetveit and T. Olsen, "Gas kick experiments in oil-based drilling muds in a full-scale, inclined research well," *SPE Annual Technical Conference and Exhibition*, 10 1989.

[23] W. Letton, J. Pappas, and J. Shen, "More improvements to deepwater subsea measurement - overview," in *Offshore Technology Conference*, OTC, 5 2015.

[24] S. Hazarika, N. Sinha, R. Bansal, and R. Jayaram, "Evaluation of single point gas lift system for a deep water oil field, india," in *SPE Oil & Gas India Conference and Exhibition*, SPE, 11 2015.

[25] D. Blakney, E. Cripps, J. Quintero, R. D. Bradshaw, A. Belloso, D. Glass, and M. Hurlburt, "Combining state-of-the-art hybrid bit and positive displacement motors saves 863,670 cad over 20 wells in northern alberta, canada," in *SPE Oklahoma City Oil and Gas Symposium*, SPE, 4 2019.

[26] S. Antal, T. Nagy, and A. Boros, "Improvement of bonded flexible pipes acc. to new api standard 17k," in *Offshore Technology Conference*, OTC, 5 2003.

[27] I. Sarsenov, A. Blackman, and S. A. M. Obeyesekere, "Papua new guinea economic update : Slower growth, better prospects," 1 2019.

[28] M. Ren, X. Li, X. Chen, and W. Ren, "Research of drilling gas kick and blowout characteristic based on the volume of fluid model," *International Journal of Digital Content Technology and its Applications*, vol. 7, pp. 797–804, 1 2013.

[29] M. Suezawa, "Hydrogen-point defect complexes in electron-irradiated c-doped and high-purity si," *Japanese Journal of Applied Physics*, vol. 38, pp. 608–610, 6 1999.

[30] Z. Rogoszinski and D. P. Hamilton, "Tilting uranus: Collisions vs. spin-orbit resonance," 4 2020.

[31] L. E. East, M. J. Rosato, M. Farabee, and B. W. McDaniel, "New multiple-interval fracture-stimulation technique without packers," in *International Petroleum Technology Conference*, IPTC, 11 2005.

[32] X. Chen, J. Yang, D. Gao, Y. Huang, Y. Li, M. Luo, and L. Wentuo, "Well control for offshore high-pressure/high-temperature highly deviated gas wells drilling: How to determine the kick tolerance?," in *IADC/SPE Asia Pacific Drilling Technology Conference and Exhibition*, SPE, 8 2018.

[33] G. Milner, “Real-time well control advisor,” *SPE Annual Technical Conference and Exhibition*, 10 1992.

[34] A. A. Nayeem, R. Venkatesan, and F. Khan, “Wellbore blowout prevention: improving safety through identification and monitoring of early kick indicators,” 11 2013.

[35] R. Rommetveit and E. H. Vefring, “Comparison of results from an advanced gas kick simulator with surface and downhole data from full scale gas kick experiments in an inclined well,” *SPE Annual Technical Conference and Exhibition*, 10 1991.

[36] A. R. Muis, A. M. Hidayat, and F. Irawan, “Floating mud-cap drilling application in exploration well accelerate reaching target depth while drilling surface hole,” in *IADC/SPE Asia Pacific Drilling Technology Conference*, SPE, 8 2016.

[37] C. Leach and P. Stanton, “Deep water development drilling from a spar,” in *Offshore Technology Conference*, OTC, 5 1999.

[38] R. Kiran, S. A. Naqavi, S. Salehi, and C. Teodoriu, “Human factors and non-technical skills: Towards an immersive simulation-based training framework for offshore drilling operations,” in *SPE Annual Technical Conference and Exhibition*, SPE, 9 2019.

[39] O. Santos, J. Mendes, and P. Ribeiro, “The development and application of a software to assist the drilling engineer during well control operations in deep and ultra deep waters,” in *SPE Latin American and Caribbean Petroleum Engineering Conference*, SPE, 4 2003.

[40] Y. Huang, J. Yang, M. Lingyu, X. Chen, M. Luo, and W. Li, “Numerical investigation on gas accumulation and gas migration in the wavy horizontal sections of horizontal gas wells,” *Mathematical Problems in Engineering*, vol. 2020, pp. 1–9, 8 2020.

[41] R. P. Santos, “Implementação de um modelo numérico para a simulação da circulação de um kick de gás pelo método do sondador,” 3 2013.

[42] J. M. Gundlach, *Section 115 in practice*. Edward Elgar Publishing, 10 2020.

[43] K. Burdin, A. Yudin, K. Ronzhin, M. Demkovich, S. G. Kreknin, K. Pushnikov, Y. Borovinskiy, and A. Zykov., “Coiled tubing advancements enable multistage stimulation and production profiling in an exploration well in eastern siberia,” in *SPE/ICoTA Coiled Tubing and Well Intervention Conference and Exhibition*, SPE, 3 2017.

[44] S. G. Karurkar, D. Chandra, and O. N. Gyani, “Development of a remote oil field through esp installation: Lessons learnt,” in *SPE Oil & Gas India Conference and Exhibition*, SPE, 11 2015.

[45] F. Kesuma, “Pengaruh kick off point terhadap perencanaan lintasan pemboran berarah pada sumur w, x, y, z,” 4 2016.

[46] D. Gomes, J. Frøyen, K. K. Fjelde, and K. S. Bjorkevoll, “Transient modelling and sensitivity analysis of influxes in backpressure mpd systems,” in *SPE Asia Pacific Oil and Gas Conference and Exhibition*, SPE, 10 2018.

[47] D. Gomes, K. S. Bjorkevoll, K. K. Fjelde, and J. Frøyen, “Numerical modelling and sensitivity analysis of gas kick migration and unloading of riser,” in *Volume 8: Polar and Arctic Sciences and Technology; Petroleum Technology*, American Society of Mechanical Engineers, 6 2019.

[48] C. S. Avelar and P. Ribeiro, “Modelagem do controle de poços por diferenças finitas,” 8 2008.

[49] K. Manikonda, A. R. Hasan, N. H. Rahmani, O. Kaldirim, C. E. Obi, J. J. Schubert, and M. A. Rahman, “A gas kick model that uses the thermodynamic approach to account for gas solubility in synthetic-based mud,” in *SPE/IADC Middle East drilling Technology conference and exhibition*, p. D031S016R001, SPE, 2021.

[50] P. L. O’Bryan, A. T. Bourgoyne, T. G. Monger, and D. P. Kopcso, “An experimental study of gas solubility in oil-based drilling fluids,” *SPE Drilling Engineering*, vol. 3, pp. 33–42, 3 1988.